Biochimica et Biophysica Acta, 1023 (1990) 325–334
Elsevier

BBAMEM 74790

Measuring changes in membrane thickness by scanning tunneling microscopy

Knute A. Fisher [1], Susan L. Whitfield [2], R.E. Thomson [2], Kathleen C. Yanagimoto [1], Mats G.L. Gustafsson [2] and John Clarke [2]

[1] *Department of Biochemistry and Biophysics and Cardiovascular Research Institute, University of California, San Francisco, CA (U.S.A.)* and [2] *Department of Physics, University of California and Center for Advanced Materials, Lawrence Berkeley Laboratory, Berkeley, CA (U.S.A.)*

(Received 22 November 1989)

Key words: Bacteriorhodopsin; Papain; Planar membrane monolayer; Purple membrane; Membrane thickness; Electron microscopy; Transmission electron microscopy; Scanning tunneling microscopy

We investigated the feasibility of using the scanning tunneling microscope (STM) as a morphometric tool to measure the thickness of biomembranes. Planar monolayers of oriented purple membrane (PM) were prepared, nitrogen-dried or freeze-etched, and coated with metal. PM thickness was quantified by STM and transmission electron microscopy. STM calibration and the effect of contamination-mediated surface deformation on measurements of PM thickness were evaluated. The thickness of PM attached to mica and glass and the effect of papain on PM thickness were also examined. The apparent thickness of enzymatically modified PM increased after papain treatment. The mean thickness of both nitrogen-dried PM on mica and freeze-etched PM on glass was 4.6 nm. After papain treatment PM thickness on mica increased to 4.8 nm and on glass to 5.4 nm. These results demonstrate that STM analysis of metal-coated planar membrane monolayers can be used to measure changes in average membrane thickness at sub-nanometer resolution.

Introduction

Methods for evaluating biomembrane and model membrane thickness include averaging techniques, such as X-ray diffraction [1], ellipsometry [2], and electrical capacitance [3], and non-averaging methods, such as light and electron microscopy. An optical leptoscope was developed in an early study to measure the thickness of the erythrocyte membrane by comparative reflectance [4]. Transmission electron microscopic (TEM) methods have utilized negative staining and grid sectioning [5], metal shadowing, and thin-sectioning of chemically fixed and stained [6] or frozen and unstained [7] samples. All techniques, whether averaging or not, face variables in membrane composition and sample preparation and are subject to limitations in instrumentation and interpretation. The present study examines the feasibility of using the STM as a morphometric tool to study membrane thickness, and specifically to evaluate the thickness of purple membrane (PM) before and after enzymatic modification with papain.

PM isolated from *Halobacterium halobium* is an ideal membrane for STM studies. PM has been extensively studied and is composed of non-glycosylated lipids and a single non-glycosylated protein, bacteriorhodopsin (bR), organized in a paracrystalline lattice [8–11]. The primary sequence of bR is known [12–14], and the structure of the membrane-spanning region has been determined to 0.28 nm resolution [15]. The size and shape of PM fragments are appropriate for STM examination. The thickness of PM has been studied by low-angle X-ray diffraction and electron microscopy. Dry membranes examined in early low-angle X-ray diffraction studies showed a stacking periodicity of 4.9 nm [16,17], and TEM micrographs of dried shadowed PM on mica revealed oval sheets 5.0 nm thick [16]. A later X-ray diffraction study showed that the axial spacing of stacked, dried PM ranged from 4.8 to 5.5 nm as a

Abbreviations: bR, bacteriorhodopsin; ES, membrane extracellular surface; HOPG, highly oriented pyrolytic graphite; *I*, electrical current; PAB, papain activating buffer; PAGE, polyacrylamide gel electrophoresis; PLG, polylysine-treated glass; PLM, polylysine-treated mica; PM, purple membrane; PS, membrane protoplasmic (cytoplasmic) surface; PZT, piezoelectric transducer; SDS, sodium dodecyl sulfate; SMM, single membrane monolayer; STM, scanning tunneling microscope or microscopy; TEM, transmission electron microscope or microscopy; *z*, vertical position of STM tip relative to sample plane.

Correspondence: K.A. Fisher, Box 0130 CVRI, University of California, San Francisco, CA 94143-0130, U.S.A.

function of pH [18]. A recent cryo-TEM study of frozen PM has determined that the phosphate headgroups are separated by 4.2 nm [19], consistent with the calculation that two, fully extended, 16-carbon acyl chains would span 4.0 nm [17]. Thermodynamic studies of PM have calculated an average thickness of 4.35 nm [20].

The goal of most biological STM studies has been to exploit the atomic resolution of the STM to gain greater detail about surface topographies [21,22]. STM analyses of biological specimens have focussed on either metal-coated samples, where resolution is limited by metal grain size, or thin, uncoated samples on conductive substrates, where lack of sample rigidity and conductivity limit resolution. To date, however, the goal of atomic resolution has not been met for biological samples, primarily due to difficulties in sample preparation (briefly reviewed in Ref. 23). Nevertheless, STM is exceptionally sensitive to displacements in z, i.e., has potentially high vertical resolution, suggesting its application to measuring the heights or thicknesses of membranes attached to and flattened against planar surfaces.

Cell monolayer and single-membrane monolayer (SMM) techniques, originally developed for electron microscopic and biochemical studies [24–30], seemed potentially well-suited to morphometric analysis by STM, especially since methods for selectively exposing the extracellular surfaces or cytoplasmic surfaces of PM had been developed [25,26,31]. SMM surfaces are composed of closely-packed, non-overlapped single membranes microscopically flat over square centimeter areas. In a preliminary study of PM thickness we reported a value of 5.3 nm [32]. In the present study conditions for calibrating the STM for use as a quantitative tool in membrane thickness studies were investigated, and further PM analyses yielded lower values of average thickness.

We also evaluated the feasibility of using STM to measure the effect of enzyme treatment on the apparent thickness of planar membranes. In PM studies, papain has been used to evaluate the topography of bR and is known to cleave at least 17 amino acids from its C-terminus [33–35]. An unexpected finding of the present study was that the apparent thickness of PM increased several Ångstroms after removal of 17–22 amino acids from the C-terminus of oriented bR.

Materials and Methods

Preparation of planar monolayers of oriented PM

Growth of *Halobacterium halobium* cultures and isolation and purification of PM were as previously described [37]. Briefly, PM was isolated from *H. halobium* by hypotonic lysis, purified on sucrose density gradients, and washed with appropriate buffers. For oriented planar monolayer preparations it was important that PM be fresh, not contaminated with bacteria, and not stored frozen in sucrose. Polylysine-treated glass (PLG) was prepared and rapidly dried with N_2 [25]. Polylysine-treated mica (PLM) was prepared from 11 mm × 22 mm strips of mica (Ted Pella, Inc. Redding, CA) freshly cleaved with a razor blade or by tape peel. Polylysine was applied for 30 s, rinsed, and dried rapidly with N_2 [23]. PM at a concentration of 3–4 mg bR/ml in 10 mM buffers, pH 3, 5, or 7, was applied to PLG or PLM while gyrating the sample for 30 s to coat its entire surface quickly (0.15 μl PM suspension /mm^2). Oriented PM monolayers with cytoplasmic surfaces (PS) exposed (> 99% PS) were prepared by applying PM in 10 mM maleic acid buffer (pH 3.0). For a mixture of orientations, with both cytoplasmic and extracellular surfaces (ES) exposed, light-adapted PM was applied in 10 mM acetate buffer (pH 5.0) for 50% ES orientation, or in 10 mM phosphate buffer (pH 7.0) for 70–90% ES orientation. PM monolayers were briefly sonicated, washed, and stored under water until needed [25].

Papain treatment of PM monolayers

Papain (Sigma Chemical Co., St. Louis, Mo, 10 mg, 14.2 units/mg) was added to 100 ml of papain activating buffer, PAB (0.01 M EDTA, 0.06 M β-mercaptoethanol, 0.05 M cysteine-HCl, 1 M NaCl, pH 6.2) and equilibrated to 37 °C for 5 min with constant rotary shaking. Oriented PM monolayers in v-racks [25] were placed in PAB with and without papain and incubated with shaking for 30 min. The reaction was stopped by rapidly overflowing reaction vessels with several volumes of distilled water, sonicating each glass for 15 s in 1 M NaCl (pH 9) to remove adsorbed papain, and rinsing with distilled water for 30 s.

For gel electrophoresis, SMM were stored in distilled water prior to solubilizing in sample buffer. For microscopy, SMM were either dried with a burst of nitrogen gas or frozen in Freon-22 and stored in liquid nitrogen until being coated or shadowed with metal [25].

SDS-polyacrylamide gel electrophoresis

Three SMM (11 × 22 mm) were blotted with filter paper and incubated in 500 μl SDS-PAGE sample buffer [38] at 75 °C for 3 min and cooled. Samples (50 μl) were applied to a 3.5% stacking gel overlying a 12.5% separation slab gel, electrophoresed, fixed, washed, and silver-stained [39].

Transmission electron microscopy

Nitrogen-dried SMM were shadowed at room temperature (approx. 20 °C). Frozen SMM were transferred from liquid nitrogen to a cold stage in a Varian VE-61 vacuum evaporator, freeze-dried (deep-etched) at −80 °C and shadowed at about −60 °C. Pt-C was

evaporated by resistance heating at $< 2 \cdot 10^{-6}$ Torr at an angle of 21°. Replicas were stripped from the glass or mica by floating onto HF, washed, transferred to grids and examined with a Siemens 101 electron microscope calibrated with crystalline catalase.

Thicknesses of control and papain-treated SMM were determined from micrographs printed at a calibrated magnification of about 350000×. The widths of electron-transparent shadows cast by single membranes at edges normal to, and distal from, the shadowing source, were measured using a 7× ocular comparator, smallest scale divisions = 0.1 mm. Widths were corrected for grain size.

Scanning tunneling microscopy

Nitrogen-dried SMM were metal coated at an angle of 90° at room temperature (approx. 20°C), and freeze-etched monolayers coated at −60°C. Pt-Ir-C [40,41] was evaporated by resistance heating at $< 2 \cdot 10^{-6}$ Torr in a Varian VE-61 vacuum evaporator. Metal-coated SMM on PLG and PLM were examined in air and in situ (left attached to the substrate) with a modified piezoelectric tube type STM [42].

Several STM tips were evaluated for bio-STM studies including etched tungsten wire with and without gold plating, and cut wire tips of Pt-Rh, Au, and Pt. Our routine tip was formed from 1.0 mm diameter $Pt_{0.9}Rh_{0.1}$ thermocouple wire (Engelhard, Carteret, NJ) cut with diagonal cutters.

The STM piezoelectric transducer (PZT) was routinely calibrated in the horizontal x and y planes by scanning freshly cleaved crystals of highly oriented pyrolytic graphite, HOPG (Union Carbide, Grade ZYB). Linear displacement of the PZT in the vertical (z) plane was calibrated by several methods. A microinch position measuring system, Model KD-2810 (Kaman Instrumentation Corp, Colorado Springs, CO), was used to measure z displacement both statistically and dynamically. For static calibrations, KD-2810 sensor position and output were calibrated against a micrometer-driven target, and regions of linear output determined. PZT measurements were taken at two voltages, −12 V and +246 V; at least three PZT measurements were taken at each of several microinch output voltages. Dynamic calibrations were obtained by modulating z with a pulse generator and recording KD-2810 output on a storage oscilloscope. Other dynamic calibrations were achieved by laser interferometry for both broad (e.g., 750 nm) and narrow (e.g., 50 nm) displacements. For internal standards, 4.9 nm colloidal gold (Jannsen Life Sci. Div., Piscataway, NJ) was applied to PLG and PLM, washed, nitrogen, dried, and metal shadowed or metal coated. Contamination-mediated surface deformation of PM on PLG was evaluated by monitoring current (I) versus tip position (s) [43] for tips positioned over PM and over substrate.

Data were acquired in the constant current (topographic) mode [44]. Unless otherwise noted, tunneling current was 3 nA and the sample was biased at +0.2 to +1.0 V. Typically we obtained 1 μm × 1 μm images of 128 lines at 256 points/line in about 6 min. For height analyses STM data was collected with a DEC LSI 11/73 computer and images corrected for average z-drift, rotated to an average flatness, and transferred to a Tektronics 6130 computer with 4129 display for analysis. Programs were written to select areas of membrane and substrate (PLG or PLM) by cursor positioning, and to calculate membrane heights by least squares fitting of two parallel planes representing membrane and substrate. STM and TEM data were evaluated using Student's t-test.

Results

TEM and STM of planar PM

TEM observations of PM on PLG were as previously reported [25,31]. Sonication removed most overlapped and folded PM producing a closely-packed single membrane monolayer (SMM). TEM observations revealed PM surfaces that ranged from smooth after freeze-drying (Fig. 1a) to cracked or pitted after nitrogen drying, representing extracellular surfaces (ES) and protoplasmic surfaces (PS), respectively [31]. Application of PM suspended in pH 3 buffer produces SMM with highly oriented PM. Previous quantitative TEM studies of air-dried shadowed SMM showed pitted membrane [25] with 99% of the ES bound, PS free. Application of PM at pH 7 produced SMM with PS preferentially adsorbed to PLG, and TEM of air-dried, shadowed SMM showed a mixture of pitted and cracked membrane. Glass and PLG surfaces were consistently rougher than mica and PLM surfaces.

Preparation of PM monolayers on PLM was less reproducible than on PLG. Although areas were similar to PM on PLG, i.e., closely-packed and non-overlapped, other areas on PLM were either devoid of membrane, minimally covered, or contained aggregated membranes. In addition, the surface morphology of PM attached to PLM (Fig. 1b) often differed from that of PM on PLG. Whereas nitrogen-dried PM on PLG was essentially smooth, nitrogen-dried PM on PLM was often pitted or finely cracked.

STM imaging of metal-coated samples was facilitated by scanning large (1 μm × 1 μm) areas. When scans were limited to 0.1 μm × 0.1 μm, sample recognition was difficult. Identification of sample and substrate was also facilitated by the thin, plate-like shape of PM (Fig. 1c). Moreover, PLM samples that were nitrogen dried occasionally showed pitted and cracked patterns similar to those seen in TEM micrographs of PLG samples after slow air drying [31]. Even without such drying artifacts, however, PM profiles could be easily and

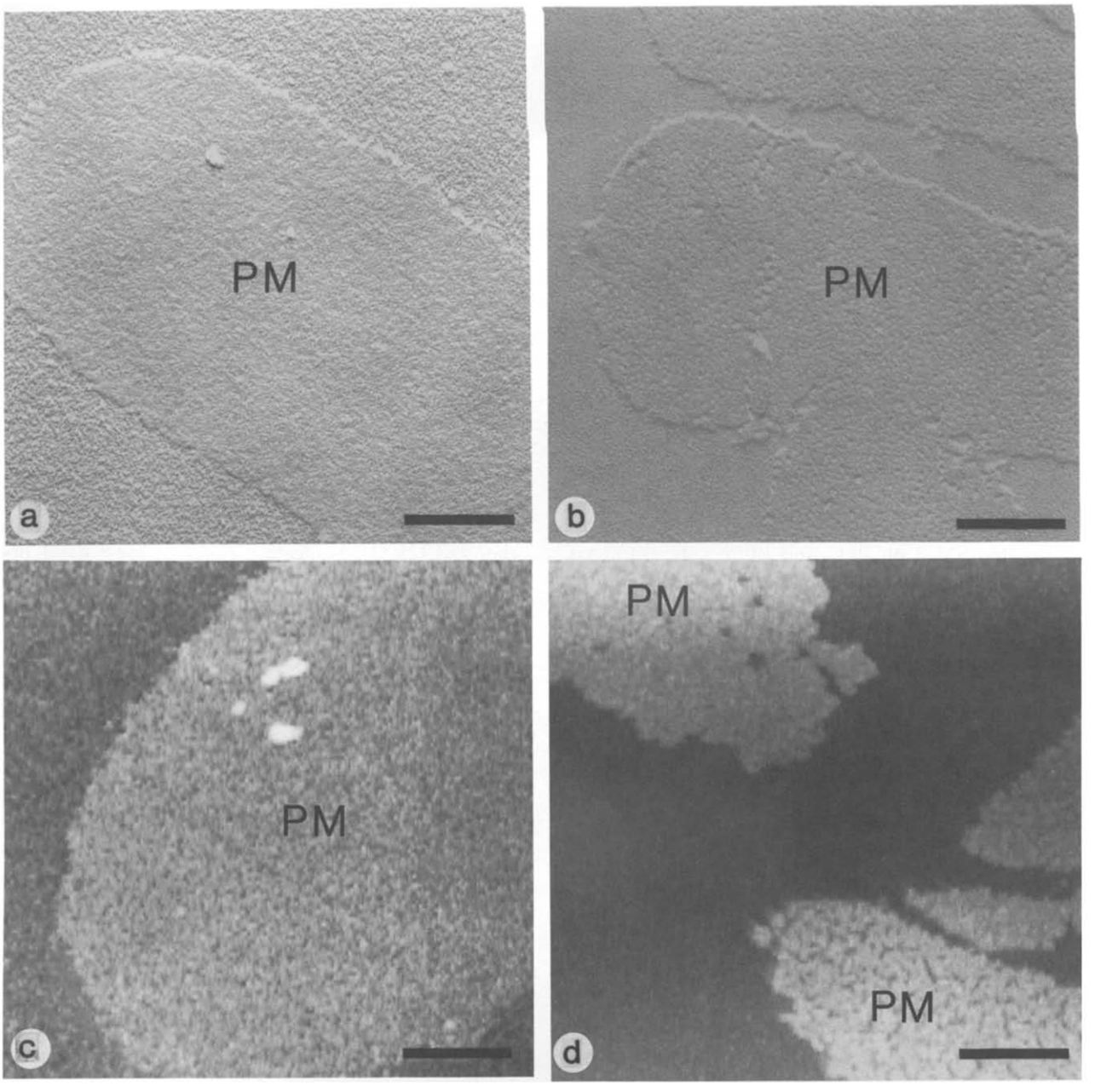

Fig. 1. TEM (a, b) and STM (c, d) images of purple membranes (PM) attached to polylysine-treated glass (a, c) and mica (b, d,). Samples on glass were freeze-dried, samples on mica nitrogen-dried. For TEM samples were shadowed with Pt-C at an angle of 21°, for SEM coated with Pt-Ir-C at an angle of 90°. Pt-Ir wire wrapped on a carbon electrode was evaporated by resistive heating and deposited at $< 2 \cdot 10^{-6}$ Torr on sample surfaces at 20° C. (c) STM image: computer processed, top-view, gray-scale representation where black = lowest point, white = highest. (d) STM image showing pitted and cracked PM surfaces. TEM shadow direction, bottom to top; STM scan direction left to right. Bars = 200 nm.

routinely recognized in projected and top-view STM images (Fig. 1c, d). Highly pitted and cracked membranes were not used for membrane thickness measurements.

Gel electrophoresis of papain-treated oriented PM monolayers

The orientation of adsorbed PM was evaluated biochemically by SDS gel electrophoresis. Silver-stained gels showed no differences in relative mobility between PM in suspension (Fig. 2a) and PM adsorbed to PLG after incubation in papain activating buffer for 30 min at 37° C (Fig. 2b, d). No differences were detected for PM oriented by application from pH 3 buffer to expose cytoplasmic surfaces (Fig. 2b) or from pH 7 buffer to expose a mixture of cytoplasmic and extracellular surfaces (Fig. 2d). Papain treatment of pH-oriented samples produced two patterns (Figs. 2c, e). Samples

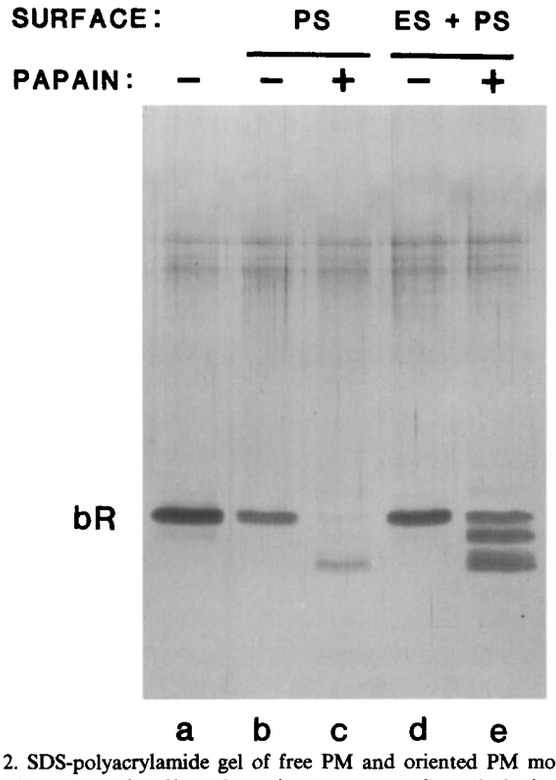

Fig. 2. SDS-polyacrylamide gel of free PM and oriented PM monolayers illustrating the effect of papain treatment on bacteriorhodopsin (bR). (a) PM suspension, 300 ng, showing a single bR band. The faint triplet bands at the top of the gel are artifacts associated with the silver-stain technique. (b, c) PM attached to PLG with the cytoplasmic surface (PS) or bR exposed, incubated with papain activating solution for 30 min at 37°C without papain (−) and with papain (+). (c) The lower molecular weight band represents papain-cleaved bR. (d, e) PM attached to PLG with a mixture of extracellular (ES) and PS surfaces adsorbed. (d) Unmodified bR. (e) bR plus its cleavage products. Lanes b–e: three 11×22 mm PM monolayers were blotted dry, added to 500 μl of sample buffer at 75°C, heated for 3 min, and cooled. Aliquots (50 μl) were applied to each lane of a 12.5% 0.75 mm thick slab gel, polypeptides separated by 5.5 h electrophoresis, and gel washed and silver stained.

with cytoplasmic surfaces exposed (applied at low pH) were uniformly cleaved producing a single lower molecular weight band (Fig. 2c). In addition, in some samples, especially on PLM (data not shown) there was a reduction in the total amount of membrane recovered after papain treatment. However the gel patterns of PM attached to PLM were the same after papain treatment as those of PM attached to PLG. Mixed orientation samples showed a mixed population of unmodified, nicked, and cleaved molecules (Fig. 2e). No bands other than bR or its papain cleavage products were observed, indicating the absence of papain or other membranes or proteins adsorbed to the surfaces of shadowed membranes and substrates.

TEM and STM of papain-treated oriented PM

TEM (Figs. 3a, c) and STM (Figs. 3b, d) images of papain-treated samples were qualitatively similar at low resolution to untreated samples. In some instances, however, papain-treated PM appeared 'smoother', i.e., had fewer pits and cracks than untreated PM (compare Fig. 3b to Fig. 1b).

TEM and STM of glass and mica substrates

TEM of metal-shadowed replicas of cover glasses and mica from several sources revealed that glass (Fig. 4a) was consistently rougher than mica (Fig. 4b). STM of metal-coated glass and mica also showed differences in roughness especially apparent in single line scans (Figs. 4c, d). The granularity observed with the STM was often variable, however, a function not only of substrate, but also of coating thickness and substrate temperature during metal condensation. Lower temperature surfaces produced smaller grains. Although mica surfaces were much smoother in both TEM and STM images, the effect of surface roughness and metal thickness on average membrane thickness measurement was minimal. Polylysine (PL) treatment of glass and mica did not significantly alter the images of those surfaces.

STM calibration of z displacement

Both static and dynamic methods were used to calibrate the vertical displacements of the PZT. Of the calibration procedures used, static measurements with the microinch position measuring system were the most variable and gave the lowest nm/V values; e.g., for the present study 2.5 nm/V. Operating the microinch system dynamically at 1 Hz gave values of 2.9 nm/V. Other dynamic measurements using laser interferometry at higher frequencies, e.g., 10 kHz, were 3.0 nm/V, and 3.1 nm/V.

Methods for using colloidal gold as an internal standard for height measurements were evaluated by TEM and STM. TEM was used to quantify the surface and size distribution of uncoated 4.9 nm colloidal gold on conductive substrates such as HOPG and Pt-C-coated mica. When TEM verified dense packing of colloidal gold, however, STM seldom showed particle images. But if IgG-coated gold was applied to PLM and coated with Pt-Ir-C, single particles and aggregates were imaged routinely by STM. Routine calibration of z was necessary during the present study since calibration decreased from 4.4 nm/V to 3.0 nm/V over a period of about 4 months.

Contamination-mediated surface deformation was evaluated from curves of tunneling current versus tip position. I/s curves taken with the STM tip positioned over metal-coated membranes were qualitatively similar to, and could be superimposed on, I/s curves taken from adjacent areas of metal-coated substrate. We concluded that deformation did occur but was comparable on sample and substrate and thus did not contribute significantly to errors in height measurements.

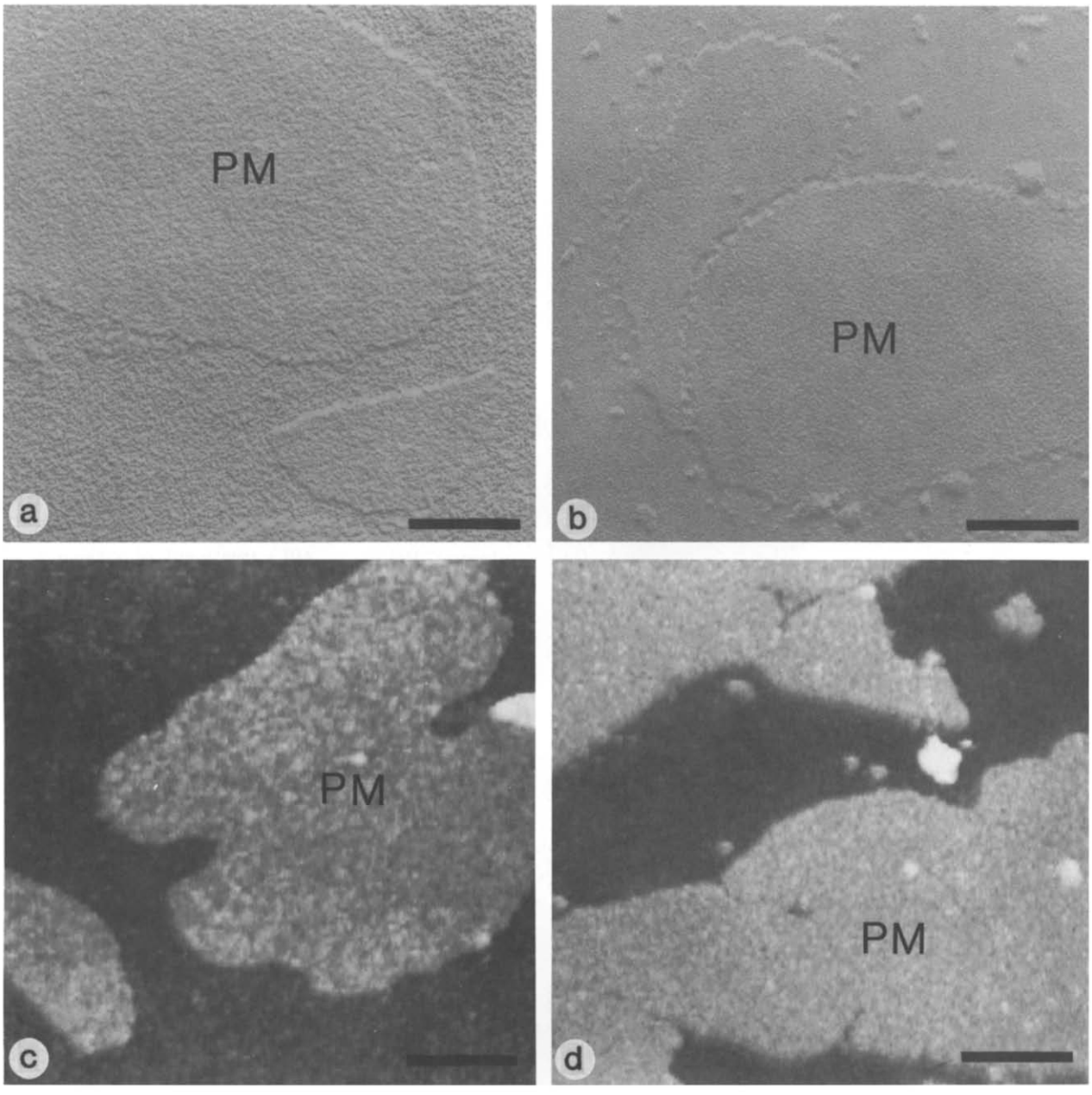

Fig. 3. TEM (a, b) and STM (c, d) images of PM on glass (a, c) and mica (b, d) after papain treatment. Sample preparation as in Fig. 1. Bars = 200 nm.

Quantification of PM thickness by STM

The thicknesses of PM adsorbed to PLG and freeze-dried, and to PLM and N_2-dried, before and after treatment with papain, were evaluated by STM and TEM. Apparent differences in membrane thickness were detected both qualitatively and quantitatively. Fig. 5 shows an STM line-scan image of PM on PLM, N_2-dried, before (Fig. 5a) and after (Fig. 5b) treatment with papain. The single line scan images (Figs. 5c, d) are selected from the images in Figs. 5a and 5b, respectively. Although single scans from a single membrane were variable, there was a reproducible difference between the apparent heights of scans of untreated versus treated PM. The upper surfaces of papain-treated membranes were consistently farther from the substrate (Fig. 5d) than the untreated membrane (Fig. 5c).

STM thermal drift, vibration, and tip/surface irregularities required that data be processed to remove z drift, flatten, and rotate images, prior to height analyses. In addition, images of isolated PM were selected for PM totally surrounded by substrate so that the average substrate plane could be calculated across the width of the membrane. Some STM images were cylindrically curved. For such images PM thickness data were repro-

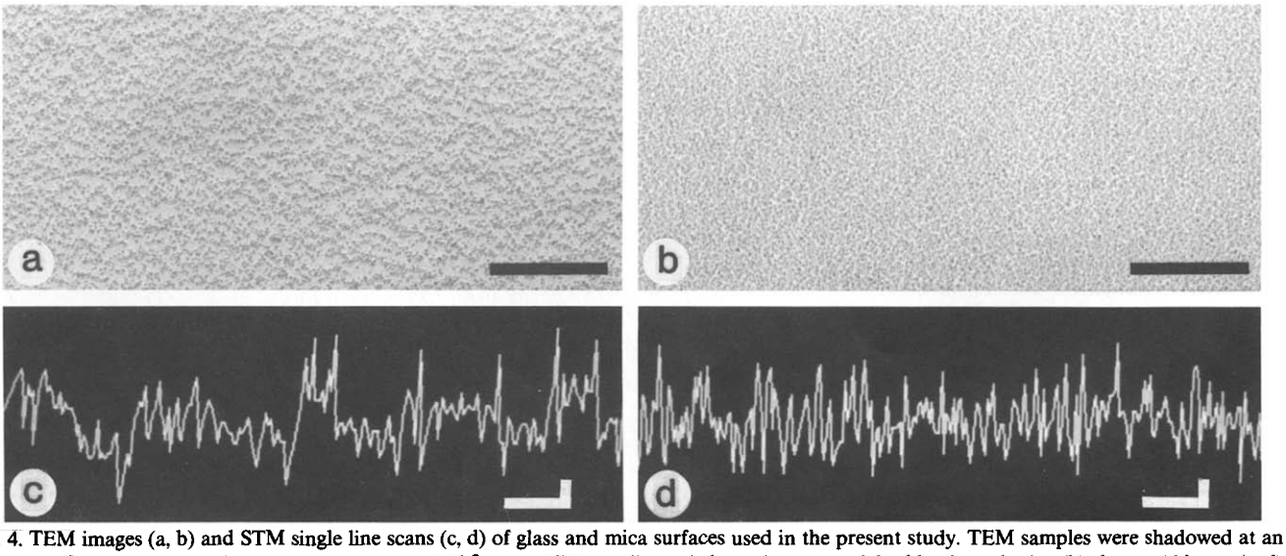

Fig. 4. TEM images (a, b) and STM single line scans (c, d) of glass and mica surfaces used in the present study. TEM samples were shadowed at an angle of 21° and STM samples coated at an angle of 90°. (a, b) TEM replicas of clean glass (a) and freshly-cleaved mica (b); bars = 100 nm. (c, d) Representative line scans of glass (c) and mica (d). Horizontal bars = 100 nm; vertical bars = 1 nm.

ducible only if adjacent regions of PM and substrate aligned with the long axis of the cylinder were evaluated. Distorted images were not evaluated, nor were PM surfaces or substrates that were contaminated, or PM that was highly pitted or cracked after N_2 drying.

Table I summarizes the results of the PM thickness measurements. STM revealed that untreated PM attached to PLG and PLM was 4.6 nm thick both after freeze-etching and after nitrogen drying. After treatment with papain, apparent mean membrane thickness

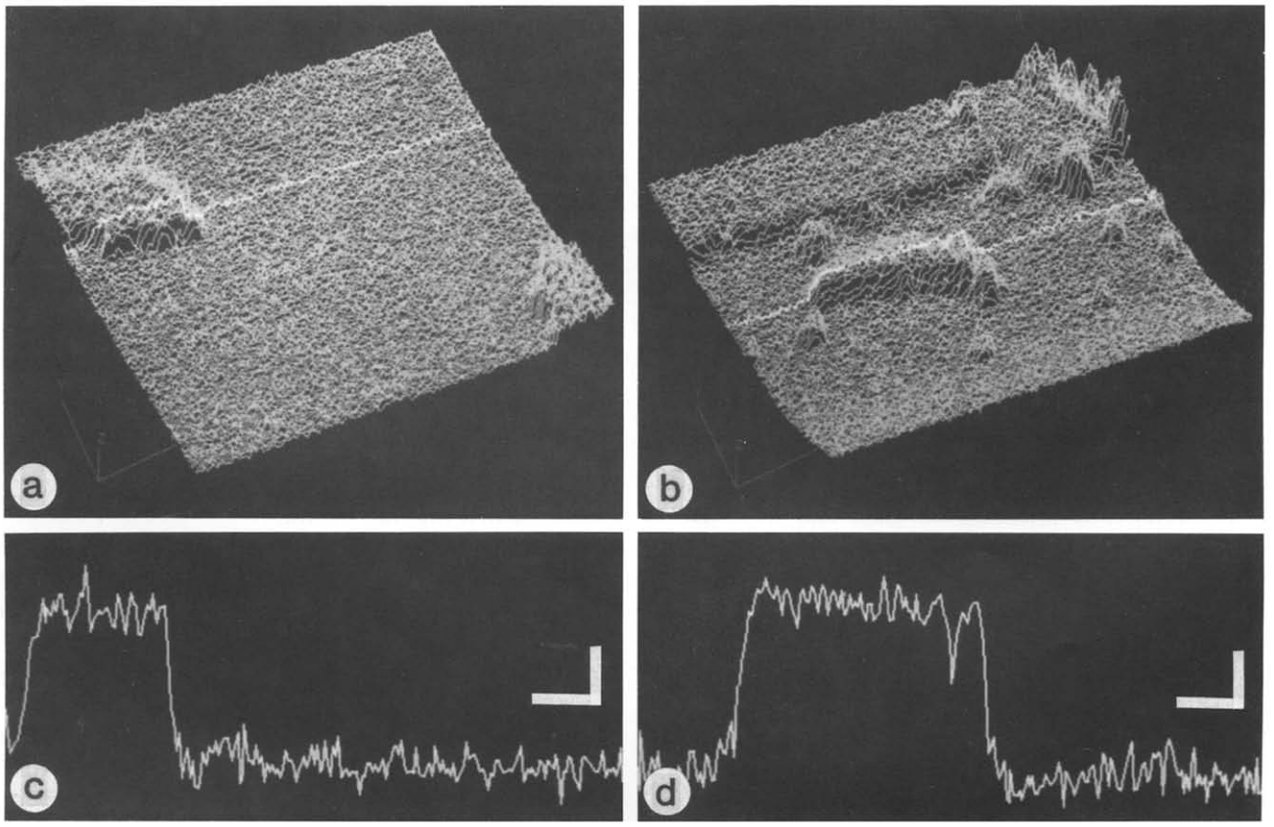

Fig. 5. STM line scan images of PM on PLM untreated (a) and treated (b) with papain. (c, d) Selected single line scans, highlighted in (a) and (b) respectively, showing signal noise in unfiltered images. Note the slight apparent increase in height (thickness) of the membrane after treatment with papain (d). (a, b) 1 μm × 1 μm area. (c, d) Horizontal bars = 100 nm; vertical bars = 2 nm.

TABLE I

Measurements of purple membrane thickness

PM were attached to polylysine-treated glass or mica, incubated in papain activating buffer for 30 min at 37°C with and without papain, either freeze-etched (F.E.) or dried with a nitrogen gun (N_2dry), and metal-coated for STM or metal-shadowed for TEM. STM thickness values were determined from calibrated average vertical displacements of z; TEM values from lengths of shadows cast by distal edges of PM normal to the shadowing source. Units are in nm given as the mean ± one standard deviation. Numbers in parentheses are number of membranes measured for each data set.

	Tunneling microscopy		Electron microscopy	
	glass-F.E.	Mica-N_2dry	glass-F.E.	Mica-N_2dry
− Papain	4.6 ± 0.4 (4)	4.6 ± 0.6 (19)	4.8 ± 0.4 (14)	4.5 ± 0.6 (13)
+ Papain	5.4 ± 0.3 (7)	4.8 ± 0.6 (12)	5.7 ± 0.5 (13)	5.3 ± 0.5 (21)

increased to 5.4 nm and 4.8 nm respectively. Student's t-distribution evaluation revealed that the increase from 4.6 nm to 5.4 nm was significantly different at the 90% confidence level. We are less than 80% confident that there is a significant difference between 4.6 nm and 4.8 nm. TEM of identical samples, shadowed at an angle of 21°, showed a thickness of 4.8 nm on PLG and 4.5 nm on PLM. Roughness of the glass surface made accurate TEM determination of the edge of the membranes and width of the shadows difficult. This uncertainty is reflected statistically in the large standard deviation of measurements of PM on glass. TEM confirmed that PLG and PLM samples were thicker after papain treatment: 5.7 nm and 5.3 nm, respectively. Student's t-distribution evaluation revealed that the increases from 4.8 nm to 5.7 nm and from 4.5 nm to 5.3 nm were both significantly different at the 99.9% confidence level.

Discussion

We have used STM to measure protease-induced changes in the apparent thickness of PM adsorbed to planar substrates. Several features of sample preparation and STM calibration were investigated. These included determining the feasibility of routinely imaging PM by STM, calibrating vertical movement of the STM tip, measuring PM thickness on glass and mica substrates after freeze-etching and nitrogen drying, and measuring the effect of papain on oriented PM monolayers by gel electrophoresis, TEM, and STM.

STM imaging of PM monolayers

TEM examination of shadowed preparations was especially important to the STM studies. TEM independently verified surface coverage and PM morphology providing confidence that STM images were topographic representations of membrane bound to substrate. Combining SMM techniques with STM made it possible to image PM with the consistency necessary for morphometric analyses; PM were readily identified by shape and size. The unique shape of each PM also facilitated identification of ghost images caused by multiple STM tips. We did not reproducibly image the bR lattice, the carboxyterminal amino acid chains, or surface extensions of the bR helices and their interconnections presumably due to the thickness of the metal coating.

STM as a morphometric tool

The STM has been used to examine both uncoated [41,45–47] and metal-coated biological samples [40,48,49]. Although the STM is capable of imaging uncoated samples, for chemically and physically heterogeneous surfaces it has been noted that "measured vertical displacements cannot be expected to correlate reliably with physical distances" [47]. Moreover, vertical displacement of the STM tip in air is a function of tip-surface distance, work function, bias potential, scan rate, PZT properties and feedback, and contamination-mediated surface deformation.

Metal-coated surfaces have several advantages for STM topographic and morphometric studies including compositional homogeneity, electrical conductivity, and immobility. Electrical conductivity is especially important since electron flux can be 10^{10} electrons/s (1 nA) in a 0.1 nm^2 area [22]. Coating the sample with metal also prevents tip-sample interactions leading to sample displacement [41,47]. In addition, for thickness or height measurements conventional low-resolution metal coating techniques are routine and convenient. We have assumed that metal thickness is not critical for z measurements as long as it is continuous and uniform in decoration and nucleation. Neither is metal grain size important if grains overlying substrate and membrane interact similarly with the STM tip; e.g., similar steric restrictions on tip penetration into narrow crevices and similar lateral tunneling between side of tip and edges of grains. One of the first applications to exploit STM z sensitivity was measurement of ripple-phase height in isolated, inverted freeze-fracture replicas of dimyristoylphosphatidylcholine [48]. Our approach differs in that we average STM z signals over large areas and examine metal-coated samples in situ.

Accurate measurement of membrane thickness required careful calibration of z displacement of the STM tip. We found dynamic calibration of z using laser interferometry to be more reproducible than static calibration using a microinch position detector. Perhaps more reliable STM vertical calibrations will be derived from internal standards, such as colloidal gold or ferritin, co-deposited with the sample prior to metal-coating. Such internal standards have the significant potential advantage of compensating for adsorbate-mediated surface deformation of samples deposited on layered substrates such as HOPG [43]. Our observations of I/s

curves of metal-coated PM on PLG as well as the comparison of STM with TEM thickness measurements showed no major influence of deformation on thickness values.

Measuring PM thickness

Sample preparation is especially important for quantitative STM studies. PM thickness has been primarily determined by X-ray diffraction and electron microscopy. A thickness of about 5.0 nm is generally assumed [16], although reported average values range from 4.2 nm to 5.8 nm. As has been shown by low-angle X-ray diffraction, sample preparation methods clearly influence apparent membrane thickness [18].

In the present study, samples were prepared from freshly purified PM applied to two polylysine-treated surfaces, cover glass and mica, either freeze-etched or nitrogen dried, and shadowed or coated with metal. Each step of PM preparation can potentially influence TEM or STM thickness measurements. For example, PM that has been stored is often contamined with bacteria. Gels of stored membranes often show multiple bands and PM applied at different pH to cationic surfaces no longer attaches selectively and predictably by one surface. The thickness of PM tethered to polylysine-treated surfaces may be influenced by the electrostatic interaction and/or thickness of polylysine sandwiched between substrate and membrane. However, the adjacent substrate is also polylysine coated and subtracted from membrane plus polylysine. Exposure to vacuum condensation of evaporated metal may also alter surface details. For STM we assume that when the metal coating is thick (e.g., > 2 nm), grain nucleation and size are not significantly different over membrane and substrate.

For STM thickness measurements we assume that variations in thickness, grain size, and grain shape of the metal coating, variations in tip/substrate and tip/membrane interactions, and variations in STM signal averaging and smoothing are the same over areas of membrane (sample) and areas of substrate (reference). This subtractive approach is analogous to the technique of difference spectroscopy. The similarity of the data for PM on two surfaces of different roughness support our assumption.

Leaving the membranes attached to the substrate in situ avoids the morphometric uncertainties inherent in TEM examination of replicas. During stripping and cleaning for TEM examination, replicas often contract and/or expand and fragment, distorted by air/solvent surface tensions. Replica perturbation is also possible during transfer to supportive films and during irradiation by the electron beam. Thickness measurements can only be made at the edge of the shadowed membrane; and it is assumed that membrane thickness at its edge is the same as at its center. Determining which portion of the distal edge of the membrane is precisely perpendicular to the shadowing source is subjective, and the precise edges of metal grains are obscured by poor focus or low contrast. Roughness of both membrane and substrate surfaces adds uncertainty to measurements of shadow width. Substrate roughness undoubtedly contributed to the large data spread, large standard deviations, of the TEM data. Our TEM measured thicknesses ranged from 4.5 nm to 5.7 nm. Finally, in practice one obtains relatively few height measurements from a TEM micrograph compared to the large number of measurements obtained by averaging the data in a single STM image.

Measuring changes in PM thickness

The minimum thickness of hydrated PM is a function of the phospholipid bilayer, approx. 4.0 nm. Furthermore, both X-ray and electron diffraction studies suggest that bR does not protrude significantly from the surface. X-ray data suggest that if bR is spherical and similar to myelin in diffraction properties, it could not protrude by more than about 0.7 nm [18]. Papain treatment for less than 1 h at papain : PM ratios of 1 : 10 cleaves 17 amino acids from the C-terminus of bR [34]. Papain treatment and polypeptides release would be expected to reduce the physical thickness of PM. However, both TEM and STM detect a slight increase in thickness regardless of conditions of sample preparation or type of substrate.

Several hypotheses can be proposed to explain the apparent increase in membrane thickness. Removal of the carboxyl-terminus from the cytoplasmic surface and/or papain nicking of bR may induce a conformational change in bR and apparent thickening of the polylysine-tethered membrane. Although this could be examined by low angle x-ray diffraction of papain-treated PM, polylysine-anchored single PM sheets may behave differently than centrifuged, stacked, and dried PM.

A second hypothesis is that PM thickness is minimally altered or even decreased by papain treatment, but that the separation between the PM and the cationic substrate is increased. Some evidence weakly supports this latter hypothesis. Release of carboxyls from the cytoplasmic surface would make PM more positively charged, putatively increasing the repulsion between PM and the cationic substrate. Less bR is recovered on SDS gels after papain cleavage suggesting that PM is lost from the PLG during washes after buffer treatment, i.e., is less tenaciously attached. Freeze-etched papain-treated membranes are apparently thicker than air-dried membranes, even on identical substrates (data not shown), suggesting that apparent thickness is a function of an etchable hydration layer between membrane and substrate. Finally, the difference in thickness between treated and untreated PM is less after nitrogen drying

than after freeze-etching, again suggesting an etchable hydration layer.

We believe this STM approach for measuring PM thickness can be applied to other membranes, for example, SMM of red blood cell membranes.

Synopsis

We have used the STM as a morphometric tool to measure small changes in the apparent thickness of PM. Although high resolution lateral details of PM surfaces were obscured by thick metal coatings, when z values were averaged over square micron areas of membrane and adjacent areas of substrate, high resolution (sub-nanometer) vertical thickness information was obtained.

Acknowledgements

We thank Mrs. Eleanor Crump for editorial help, and Drs. Paul Hansma, Stuart Lindsay, and Walther Stoeckenius for helpful comments. This work was supported by National Institutes of Health Grant DA 05043 (K.A.F.) and by the Director, Office of Energy Research, Office of Basic Energy Science, Materials Science Division of the U.S. Department of Energy, under contract No. DE-AC03-76F00098 (J.C.).

References

1 Caspar, D.L.D. and Kirschner, D.A. (1971) Nature New Biol. 231, 46–52.
2 Rothen, A. (1945) Science 102, 446–447.
3 Benz, R., Frohlich, O., Läuger, P. and Montal, M. (1975) Biochim. Biophys. Acta 394, 323–334.
4 Waugh, D.F. and Schmitt, F.O. (1940) Cold Spring Harbor Symp. Quant. Biol. 8, 233–244.
5 Sosinsky, G.E., Jesior, J.C., Caspar, D.L.D. and Goodenough, D.A. (1988) Biophys. J. 53, 709–722.
6 Sjostrand, F.S. (1963) J. Ultrastruct. Res. 9, 340–361.
7 Lyon, M.K. and Unwin, P.N. (1988) J. Cell Biol. 106, 1515–1523.
8 Stoeckenius, W. (1985) Trends Biochem. Sci. 10, 483–486.
9 Ovchinnikov, Yu.A. (1987) Photochem. Photobiol. 45, 909–914.
10 Khorana, H.G. (1988) J. Biol. Chem. 263, 7439–7442.
11 Oesterhelt, D. and Tittor, J. (1989) Trends Biochem. Sci. 14, 31–35.
12 Ovchinnikov, Yu.A., Abdulaev, N.G., Feigina, M.Yu., Kiselev, A.V., Lobanov, N.A. and Nasimov, I.V. (1978) Bioorg. Khim. 4, 1573–1574.
13 Ovchinnikov, Yu.A., Abdulaev, N.G., Feigina, M.Yu., Kiselev, A.V. and Lobanov, N.A. (1979) FEBS Lett. 100, 219–224.
14 Khorana, H.G., Gerber, G.E., Herlihy, W.C., Gray, C.P., Anderegg, R.J., Hihei, K. and Biemann, K. (1979) Proc. Natl. Acad. Sci. U.S.A. 76, 5046–5050.
15 Baldwin, J.M., Henderson, R., Beckman, E. and Zemlin, F. (1988) J. Mol. Biol. 202, 585–591.
16 Blaurock, A.E. and Stoeckenius, W. (1971) Nature New Biol. 233, 152–155.
17 Blaurock, A.E. (1975) J. Mol. Biol. 93, 139–158.
18 Henderson, R. (1975) J. Mol. Biol. 93, 123–138.
19 Sakata, K., Fujiyoshi, Y., Morikawa, K. and Kimura, Y. (1989) Protein Eng., in press.
20 Tristram-Nagle, S., Yang, C.-P. and Nagle, J.F. (1986) Biochim. Biophys. Acta 854, 58–66.
21 Hansma, P.K., Elings, V.B., Marti, O. and Bracker, C.E. (1988) Science 242, 209–216.
22 Zasadzinski, J.A.N. (1989) Biotechniques 7, 174–187.
23 Fisher, K.A. (1989) J. Electron Microsc. Tech. 13, 355–371.
24 Fisher, K.A. (1980) Annu. Rev. Physiol. 42, 261–273.
25 Fisher, K.A. (1982) Meth. Enzymol. 88, 230–235.
26 Fisher, K.A. (1987) in Advances in Cell Biology (Miller, K.R., ed.), Vol. 1, pp. 1–29, JAI Press, Greenwich.
27 Fisher, K.A. (1989) in Freeze Fracture Studies of Membranes (Hui, S., ed.), pp. 11–39, CRC Press, Boca Raton.
28 Nermut, M.V. (1982) Eur. J. Cell Biol. 28, 160–172.
29 Nermut, M.V. (1983) Trends Biochem. Sci. 8, 303–306.
30 Edwards, H.H., Mueller, T.J. and Morrison, M. (1979) Science 203, 1343–1345.
31 Fisher, K.A., Yanagimoto, K.C. and Stoeckenius, W. (1978) J. Cell Biol. 77, 611–621.
32 Fisher, K.A., Whitfield, S., Thomson, R.E., Yanagimoto, K., Gustaffson, M. and Clarke, J. (1989) Proc. 47th Annu. Meet. Electron Microsc. Soc. Am., pp. 14–15, San Francisco Press, Inc., San Francisco.
33 Ovchinnikov, Yu.A. (1987) Trends Biochem. Sci. 12, 434–438.
34 Ovchinnikov, Yu.A., Abdulaev, N.G. and Kieslev, A.V. (1984) Biol. Membr. 5, 197–220.
35 Ovchinnikov, Yu.A., Abdulaev, N.G., Feigina, M.Yu., Kiselev, A.V. and Lobanov, N.A. (1977) FEBS Lett. 84, 1–4.
36 Abdulaev, N.G., Feigina, M.Yu., Kiselev, A.V., Ovchinnikov, Yu.A., Drachev, L.A., Kaulen, A.D., Khitrina, L.U. and Skulachev, V.P. (1978) FEBS Lett. 90, 190–194.
37 Oesterhelt, D. and Stoeckenius, W. (1974) Meth. Enzymol. 31, 667–678.
38 Laemmli, U.K. (1970) Nature 227, 680–685.
39 Fisher, K.A. and Yanagimoto, K.C. (1988) Biochim. Biophys. Acta 970, 39–50.
40 Amrein, M., Stasizk, A., Gross, H., Stoll, E. and Travaglini, G. (1988) Science 240, 514–516.
41 Amrein, M., Durr, R., Stasiak, A., Gross, H. and Travaglini, G. (1989) Science 243, 1708–1711.
42 Thomson, R.E., Walter, U., Ganz, E., Clarke, J., Zettl, A., Rauch, P. and DiSalvo, F.J. (1988) Phys. Rev. B 38, 10734–10743.
43 Mamin, H.J., Ganz, E., Abraham, D.W., Thomson, R.E. and Clarke, J. (1986) Phys. Rev. B 34, 9015–9018.
44 Hansma, P.K. and Tersoff, J. (1987) J. Appl. Phys. 61, R1–R23.
45 Drake, B., Sonnenfeld, R., Schneir, J., Hansma, P.K., Slough, G. and Coleman, R.V. (1986) Rev. Sci. Instrum. 57, 441–445.
46 Lindsay, S.M. and Barris, B. (1988) J. Vac. Sci. Technol. 6, 544–547.
47 Lee, C., Arscott, P.G., Bloomfield, V.A. and Evans, D.F. (1989) Science 244, 475–477.
48 Zasadzinski, J.A.N., Schneir, J., Gurley, J., Elings, V. and Hansma, P.K. (1988) Science 239, 1013–1015.
49 Guckenberger, R., Kosslinger, C., Gatz, R., Brev, H., Levai, N. and Baumeister, W. (1988) Ultramicroscopy 25, 111–122.